JACS
JOURNAL OF THE AMERICAN CHEMICAL SOCIETY
pubs.acs.org/JACS
Article

Pumping Small Molecules Selectively through an Energy-Assisted Assembling Process at Nonequilibrium States

Huimin Fu,[§] Nengjie Cao,[§] Wang Zeng, Min Liao, Shenglin Yao, Jiajia Zhou,* and Wei Zhang*

Cite This: J. Am. Chem. Soc. 2024, 146, 3323−3330
Read Online
ACCESS | Metrics & More | Article Recommendations | Supporting Information

ABSTRACT: In living organisms, precise control over the spatial and temporal distribution of molecules, including pheromones, is crucial. This level of control is equally important for the development of artificial active materials. In this study, we successfully controlled the distribution of small molecules in the system at nonequilibrium states by actively transporting them, even against the apparent concentration gradient, with high selectivity. As a demonstration, in the aqueous solution of acid orange (AO7) and $TMC_{10}COOH$, we found that AO7 molecules can coassemble with transient anhydride $(TMC_{10}CO)_2O$ to form larger assemblies in the presence of chemical fuel 1-ethyl-3-(3-(dimethylamino)propyl) carbodiimide hydrochloride (EDC). This led to a decrease in local free AO7 concentration and caused AO7 molecules from other locations in the solution to move toward the assemblies. Consequently, AO7 accumulates at the location where EDC was injected. By continuously injecting EDC, we could maintain a stable high value of the apparent AO7 concentration at the injection point. We also observed that this process which operated at nonequilibrium states exhibited high selectivity.

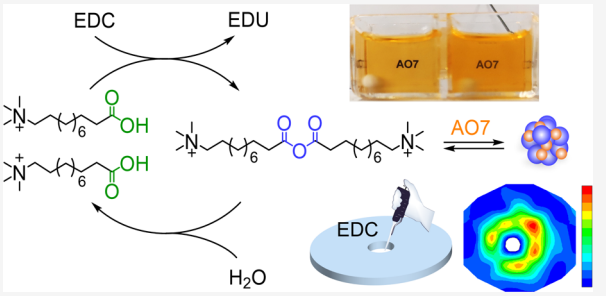

INTRODUCTION

Active materials are a class of matter that exhibit emergent properties similar to living systems, fueled by their consumption of energy.[1] These properties include the ability to adapt and dynamically respond to environmental changes and even reproduce themselves.[2] However, to achieve these properties in artificial systems, controlling the matter distribution with spatiotemporal accuracy is crucial.[3] Such active materials fall under the category of out-of-equilibrium systems from a thermodynamics perspective. While nonuniform concentration distribution of matter can be generated in equilibrium states with the aid of external fields, controlling it at nonequilibrium remains a challenge. To address this, Prins's group reported that by using a hydrogel as a reaction medium, they are able to accumulate the assemblies with large sizes trapped in a hydrogel framework through the local injection of chemicals.[4] Nature, on the other hand, employs sophisticated biostructures to selectively manipulate the concentration of small molecules. For instance, using carrier proteins fueled by ATP consumption, biological systems are able to create vital concentration gradients such as the Na^+ and K^+ gradients across cell membranes.[5] Building on this inspiration, we present an artificial carrier that can selectively load and release small molecules in response to the presence of chemical fuel. Such a system allows for the regulation of molecular diffusion, effective management of matter distribution, and the preservation of concentration differences across membranes selectively.

We propose to use surfactant $TMC_{10}COOH$, which is a carboxylic acid carrying an ammonium salt at its termini to regulate the distribution of small molecules (Figure 1a). It is well-established that carboxylic acid undergoes a dehydration reaction in the presence of 1-ethyl-3-(3-(dimethylamino)-propyl) carbodiimide hydrochloride (EDC) and forms the corresponding anhydride, which hydrolyzes back into carboxylic acid again when EDC is depleted in aqueous solution, as reported by Boekhoven,[6] Hartley,[7] and other groups.[8] In the meantime, surfactants with chemical structures similar to $TMC_{10}COOH$ will coassemble with molecules carrying negative charges to form micelles above their critical concentration.[9] It should be noted that $(TMC_{10}CO)_2O$ possesses a longer hydrophobic chain and has a lower critical concentration compared to $TMC_{10}COOH$. Taking advantage of these properties, at an appropriate concentration, we can expect $(TMC_{10}CO)_2O$ to coassemble with other molecules, such as acid orange (AO7) to form micellar structures, while $TMC_{10}COOH$ still dissolves in the solution. By utilizing the reaction cycle between EDC and $TMC_{10}COOH$, we are able to load AO7 into the assemblies with larger sizes in the

Received: November 1, 2023
Revised: January 11, 2024
Accepted: January 12, 2024
Published: January 26, 2024

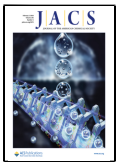

https://doi.org/10.1021/jacs.3c12228
J. Am. Chem. Soc. 2024, 146, 3323−3330

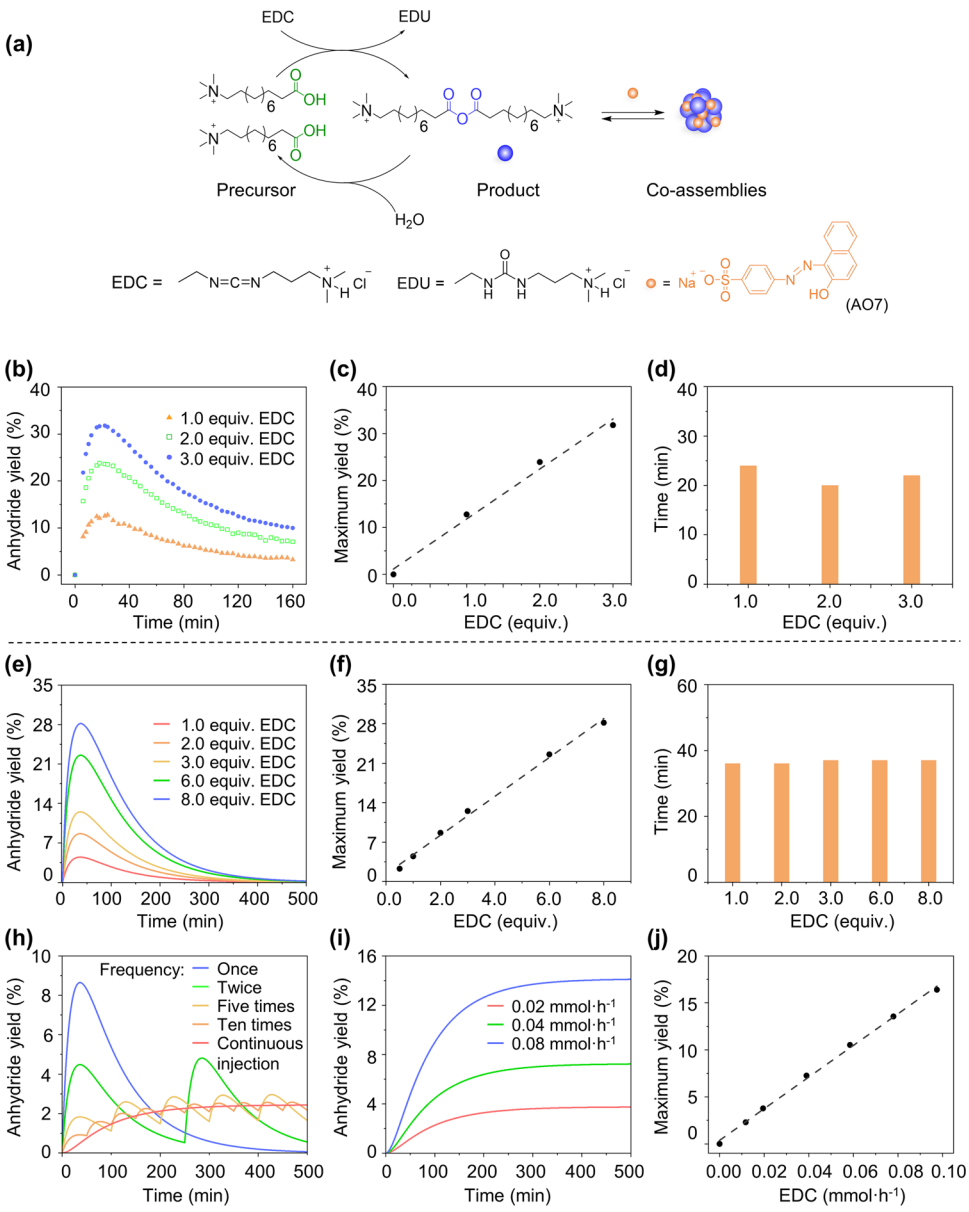

Figure 1. (a) Chemical reaction network employed to drive the product coassemble with AO7. The carboxylate group on the precursor reacts with EDC to form a transient anhydride (product). (b) Yields of anhydride against the time with varying EDC amounts monitored by ^{1}H NMR. (c) Plot of the maximum yield of anhydride against the amount of EDC. (d) Time at the maximum yield of anhydride against the amount of EDC. (e) Simulated kinetic traces of the precursor (8.0 mM) with varying EDC amounts. (f) Plot of the maximum yield of anhydride against the amount of EDC from theoretical simulation. (g) Time at the maximum yield of anhydride against the amount of EDC from theoretical simulation. (h) Yields of anhydride against the time when EDC (16 mM) was added into the solution of the precursor (8.0 mM) in 500 min. The frequency of EDC supplied was once (blue curve), twice (green curve), five times (yellow curve), ten times (orange curve), or continuous injection (red curve). (i) Yields of anhydride against the time with varying injection rates of EDC. (j) Plot of the maximum yield of anhydride after reaching steady states against the rate of EDC addition. Please note that the spherical assembled structure in the cartoon does not represent the actual structure of the assembled micelle.

presence of chemical fuel EDC and release them into the solution again after the complete consumption of EDC. This dynamic process allows us to tune the local concentration of AO7 instantaneously, enabling the generation of a concentration gradient in the solution through EDC fuel injection.

RESULTS AND DISCUSSION

Reaction Cycle in the Continuous Supply of Chemical Fuel EDC. We first confirmed that, during the reaction cycle between EDC and $TMC_{10}COOH$, we were able to maintain the concentration of transient product $(TMC_{10}CO)_2O$ at a steady value, if the chemical fuel EDC was injected in a continuous manner. When EDC (2.0×10^{-5} mol, 2.0 equiv) was added into the aqueous solution of $TMC_{10}COOH$ (1.0×10^{-5} mol in 0.5 mL D_2O, 20 mM), the reaction between them (Figure S1, see the Supporting Information for details) will lead to the formation of transient anhydride $(TMC_{10}CO)_2O$ with a maximum yield of 24% at around 20 min (Figure 1b) and then hydrolyze to form original $TMC_{10}COOH$ again. The maximum yield of $(TMC_{10}CO)_2O$ was positively correlated to the total amount of EDC in the process (Figure 1c). We also confirmed that this result matched our theoretical simulation

https://doi.org/10.1021/jacs.3c12228
J. Am. Chem. Soc. 2024, 146, 3323−3330

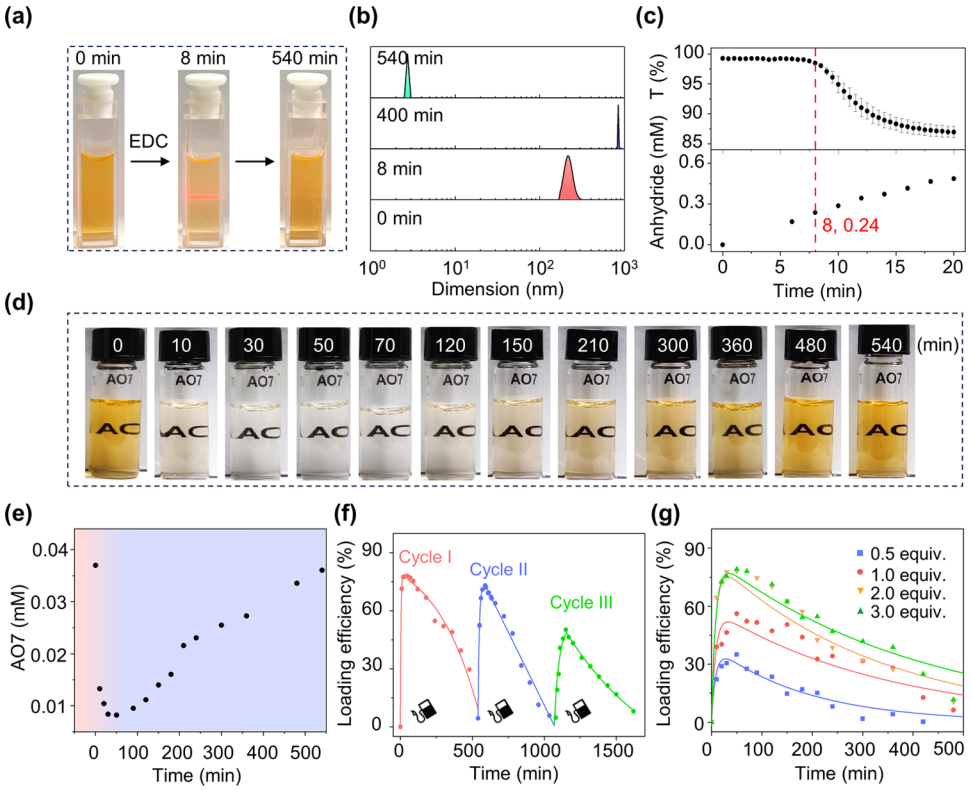

Figure 2. (a) Photographs of the reaction mixture of the $TMC_{10}COOH$ and AO7 after adding EDC at different moments. (b) Time-dependent size distribution of the reaction mixture after the addition of EDC monitored by DLS spectroscopy. (c) Time-dependent transmittance of the solution after adding EDC (top) and the concentration of anhydride (down) monitored by UV−vis spectroscopy and ^{1}H NMR spectroscopy, respectively. (d) Photographs of the filtrates at different periods after removing the assembled AO7 through filtration. (e) Concentration of AO7 in the filtrates as a function of time monitored by UV−vis spectroscopy. (f) Time-dependent loading efficiency of AO7 in the assemblies upon the addition of EDC multiple times to the aqueous solution containing $TMC_{10}COOH$ and AO7 measured by UV−vis spectroscopy. (g) Time-dependent loading efficiency of AO7 in the assemblies after varying the dosage of chemical fuel EDC.

(see the Supporting Information for details) at different conditions very well (e.g., simulation result of $TMC_{10}COOH$ at 20.0 mM, see Figures S2−S4; simulation result of $TMC_{10}COOH$ at 8.0 mM, see Figures 1e−g and S5). Ideally, when the same amount of EDC (0.104 mmol in 6.5 mL, 16 mM) was divided into two equal portions and supplied at an interval of 250 min (Figure S6), we will find two maximum yields of $(TMC_{10}CO)_2O$ (Figure 1h, green curve). One can anticipate that each extra supplied EDC (Figures S7 and S8) will generate an additional peak value of $(TMC_{10}CO)_2O$ formation (Figure 1h, yellow and orange curves). When the time intervals between each batch of EDC were negligible, which means that EDC was injected in a continuous manner (0.012 mmol·h^{-1}, Figure S9), the peak values of $(TMC_{10}CO)_2O$ production will close to a continuous manner (Figure 1h, red curve). In other words, the amount of as-formed $(TMC_{10}CO)_2O$ will reach a steady plateau under these circumstances. A further study reveals that, when the injection rate of EDC was increased from 0.02 mmol·h^{-1} (Figures 1i and S10, red curve) to 0.04 mmol·h^{-1} (Figures 1i and S10, green curve) and 0.08 mmol·h^{-1} (Figures 1i and S10, blue curve), the yields of $(TMC_{10}CO)_2O$ after reaching steady states will increase from 4 to 7 and 14%, accordingly. This result suggests that we could tune the concentration of anhydride $(TMC_{10}CO)_2O$ in the system through the supply rate of EDC at a nonequilibrium state (Figure 1j).

Loading and Releasing AO7 during the Reaction Cycle between $TMC_{10}COOH$ and EDC. The resulting transient anhydride $(TMC_{10}CO)_2O$ bearing positively charged trimethylammonium termini was able to coassemble with AO7, which carries negative charges in situ during this reaction cycle. To illustrate, we added AO7 (1.1×10^{-7} mol, 0.038 mM) into an MES buffer solution (pH 5.5, 3.0 mL, 200 mM) containing EDC (9.2 mg, 4.8×10^{-5} mol) and $TMC_{10}COOH$ (2.4×10^{-5} mol, 8.0 mM) in a quartz cuvette. We found that the initially transparent solution turned into a turbid suspension after approximately 8 min and gradually returned to a transparent state (Figure 2a). Using dynamic light scattering (DLS) spectroscopy, we did not detect any visible peak before adding EDC. However, around 8 min after the addition of EDC, we could observe the formation of particles with sizes at hundreds of nanometers in the system, which persisted for approximately 400 min and completely disappeared after 540 min (Figure 2b). However, in a control experiment without the presence of AO7, we did not observe the formation of nanoparticles. This clearly demonstrated the formation of coassemblies between $(TMC_{10}CO)_2O$ and AO7. From optical microscopy, atomic force microscopy (AFM), scanning electron microscopy (SEM), and transmission electron microscopy (TEM), we confirmed the formation of aggregated assemblies (Figures S11a−d). Using in situ bright-field microscopy, we could capture the dynamic growth process of micellar bundles (Figures S11e−h). By monitoring the time-dependent transmittance of the solution after adding EDC using UV−vis spectroscopy, we found a clear transition point at 8 min (Figure 2c, top), which indicates the critical concentration of

https://doi.org/10.1021/jacs.3c12228
J. Am. Chem. Soc. 2024, 146, 3323−3330

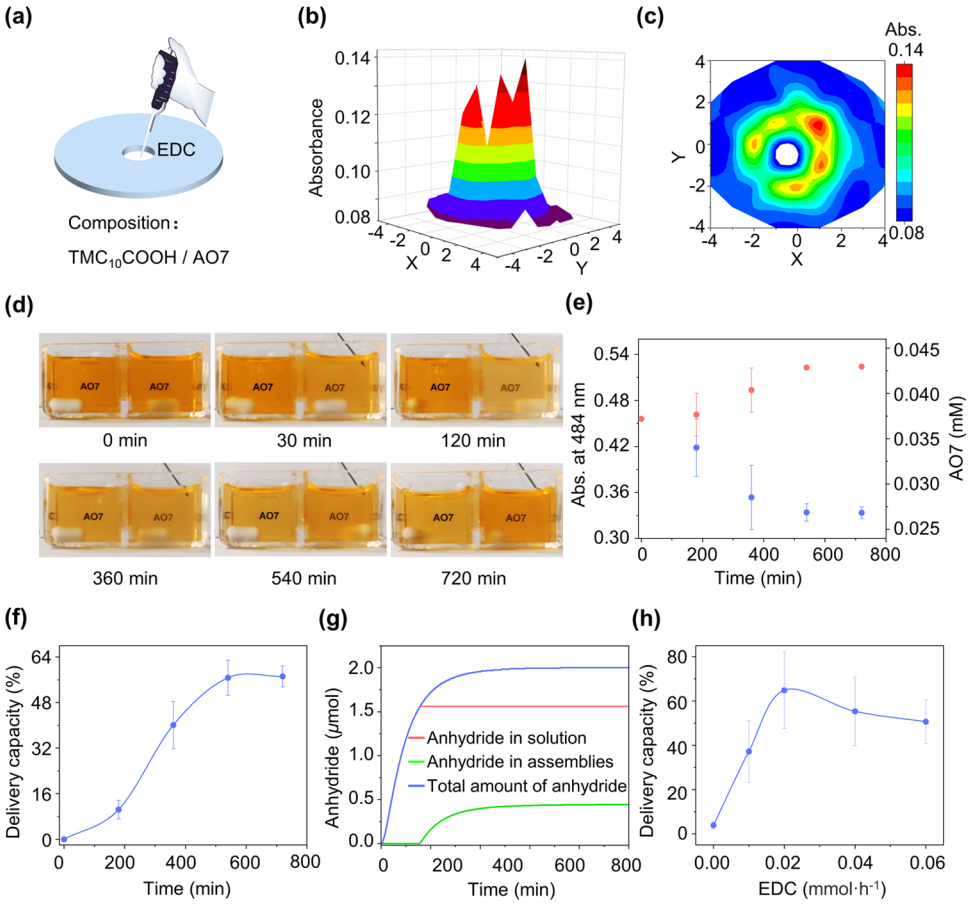

Figure 3. (a) Geometrical representation of the gel used in this work. The chemical fuel EDC was added into the center spot of the gel. (b) 3D plot of the absorbance at 484 nm in the gel at t = 60 min after the addition of EDC. (c) 2D plot of the absorbance at 484 nm in the entire gel at t = 60 min after the addition of EDC. (d) Photographs of the two-cell container at different times after the injection of EDC into the right side cell. (e) Time-dependent absorbance at 484 nm and the total concentration of AO7 of left side (blue dot) and right side (red dot) cells. (f) Plot of the delivery capacity of AO7 from the left side cell to another against the time. (g) Evolution of the amount of anhydride in the right side cell during the continuous injection of EDC calculated by kinetic models. (h) Plot of the delivery capacity of AO7 from one cell to another with EDC injection against the injection rate of EDC.

$(TMC_{10}CO)_2O$ when the coassemblies start to form. Using time-dependent ^{1}H NMR, we were able to determine that the concentration of $(TMC_{10}CO)_2O$ at this moment was 0.24 mM (Figure 2c, down).

We also found that during the reaction cycle between $TMC_{10}COOH$ and EDC, along with the formation and hydrolysis of anhydride $(TMC_{10}CO)_2O$, small molecules AO7 could coassemble with $(TMC_{10}CO)_2O$ and be released to solution in the process of disassembling. Due to the relatively larger size of the assembled states, we were able to monitor the concentration of unassembled AO7 in the solution after removing the assembled AO7 through filtration. For instance, we first added EDC (4.8×10^{-5} mol, 2.0 equiv) into 3.0 mL of MES buffer (pH 5.5, 200 mM) containing $TMC_{10}COOH$ (2.4×10^{-5} mol, 8.0 mM) and AO7 (1.1×10^{-7} mol, 0.038 mM). After keeping the mixture at 25 °C for different periods of time, the mixture was filtered by using a filter membrane with 0.45 μm pore size to remove the assembled nanoparticles. We found that the color of the obtained filtrate changed from orange to light orange and colorless in the first 50 min, and then changed back to orange color in the next 540 min, indicating the different residual amounts of AO7 in the solution (Figure 2d). From their ultraviolet−visible (UV−vis) spectra, all filtrates showed a typical absorption spectrum of AO7 (Figure S12). Meanwhile, the intensity of the maximum absorption peak at 484 nm gradually decreased in the first 50 min and then increased and returned to its original state within ~540 min (Figure S12). Using the intensity of the maximum absorption peak, we were able to determine the concentration of AO7 in the solution quantitatively. By plotting the concentration of AO7 in the filtrates over time, we could clearly observe a minimum concentration of AO7 of 8.2×10^{-3} mM in the solution at 50 min, indicating that a maximum ratio of AO7 (78%) was loaded into the assembled states at 50 min (Figure 2e).

Subsequently, we found that loading and releasing AO7 could be repeated in consecutive cycles upon adding additional EDC as a chemical fuel multiple times. As shown in Figure 2f, upon adding EDC (2.0 equiv) for the first time, the percentage of AO7 in the assemblies increased to 78% in 50 min and gradually decreased to 4% after 540 min. When another batch of EDC was added into the solution, once again, we observed that the percentage of AO7 in the assemblies increased to 72% in 50 min and gradually decreased to 5% after 540 min. In the third cycle, maximum percentage of AO7 in the assemblies was found to be 50%, probably due to the fatigue caused by EDU waste.[10]

https://doi.org/10.1021/jacs.3c12228
J. Am. Chem. Soc. 2024, 146, 3323−3330

Moreover, we were able to control the loading efficiency of AO7 by varying the dosage of chemical fuel EDC. As shown in Figure 2g, if the initial dosage of EDC was decreased to 1.2×10^{-5} mol (0.5 equiv), at 50 min, we could still observe a maximum loading efficiency at 35%. When different amounts of EDC (from 0.5 equiv to 3.0 equiv vs precursor) were added to the solution of $TMC_{10}COOH$ (2.4×10^{-5} mol, 8.0 mM) and AO7 (1.1×10^{-7} mol, 0.038 mM), we found in all cases that, after 50 min, the content of AO7 in the assemblies reached the maximum with different values at 35% for 0.5 equiv EDC, 56% for 1.0 equiv EDC, 78% for 2.0 equiv EDC, and 79% for 3.0 equiv EDC.

Pumping Small Molecule AO7 at Nonequilibrium States. Utilizing this feature, we were able to manipulate the distribution of small molecules carrying negative charges such as AO7 by the consumption of chemical fuel. Using a polyacrylamide (PAM) hydrogel (see the Supporting Information for sample preparation details) as a reaction medium, we were able to visualize this process clearly. For instance, starting with a PAM hydrogel soaked with AO7 dyes, 0.01 mL of a concentrated stock solution of EDC (6.8 M) was added into the center spot of the hydrogel (Figure 3a). After that, we could clearly observe that the orange dye molecules AO7 were moving toward the center of the hydrogel. By using a microplate reader, we were able to plot the absorption intensity at 484 nm vs position and map the overall distribution of the AO7 in the whole hydrogel. As shown in Figures 3b,c and S13, 60 min after the addition of EDC, the absorbance of AO7 close to the location where EDC was added is much larger compared to other parts of the gel, indicating that the distribution of AO7 was inhomogeneous and AO7 tended to move toward regions where EDC was supplied.

In order to get more insight into this process in a quantitative way, we conducted the experiment in solution, utilizing a two-cell container separated by a microporous membrane with a pore size of 0.45 μm (Figure 3d). In this experimental setup, only small molecules were able to pass through the membrane through diffusion, while convection between the left and right cells was prohibited. Each cell was filled with $TMC_{10}COOH$ (8.0 mM) and AO7 (0.038 mM) aqueous solution (6.0/6.5 mL) containing MES buffer (200 mM, pH 5.5), respectively. Then, EDC (2.0×10^3 mM in H_2O) was continuously injected into the right side cell with a microfluidic syringe at the rate of 0.04 mmol·h^{-1}. In the first 120 min, the color of the right cell became lighter due to the free AO7 in solution being loaded into the assemblies. Then, the color of the left cell went lighter as well, caused by the diffusion of free AO7 from the left side to the right side cell. From 540 min, we could clearly observe that the cell on the right side showed a darker color than the cell on the left side. By plotting the absorption intensity at 484 nm vs time, we were able to obtain the total concentration of the AO7 (including the ones dissolved in solution and loaded in the assemblies) of each cell. As shown in Figure 3e, at the initial stage, both left and right side cells showed an absorbance equal to 0.45 at 484 nm. Along with the continuous injection of EDC fuel, the absorbance of the left side cell gradually decreased and maintained at 0.33 after 540 min. In the meantime, the absorbance of the right side cell gradually increased to 0.52. Here, we used the amount of AO7 in the right cell over the amount of AO7 in the left cell to denote the capacity to deliver AO7 from one cell to another. By comparing the total concentration of AO7 in the left (Figure 3e, blue dots) and right cells (Figure 3e, red dots) at different times (Table S1), we could clearly find that the delivery capacity increased in the beginning and reached a plateau at 57% (Figure 3f). These results unambiguously demonstrated that AO7 molecules in the left side cell were diffusing through the membrane in between two cells and accumulated in the right side cell over time. This means that using the continuous injection of EDC fuel, we were able to maintain a higher concentration of AO7 on the side where EDC was injected. In other words, in the presence of transient $(TMC_{10}CO)_2O$ as an artificial dynamic vessel, we were able to control the distribution of small molecules, such as AO7 in the system by continuous chemical energy input. Additionally, after approximately 12 h of withdrawing EDC, the solution color in both cells would be identical (Figure S14).

These results could be well supported by theoretical simulations (see the Supporting Information for details of the theoretical model). As shown in Figures 3g and S15, during the continuous injection of EDC, the anhydride $(TMC_{10}CO)_2O$ in the solution will maintain its critical concentration, while the amount of $(TMC_{10}CO)_2O$ in the assembled states started to increase after a threshold and reached a plateau eventually over time. Considering that the AO7 in the assembled states was positively correlated to the amount of coassemblies, we could conclude that the ability to deliver AO7 through EDC injection came from that continuous injection of EDC would maintain a stable amount of anhydride $(TMC_{10}CO)_2O$ in the assembled states.

Moreover, the ability to deliver AO7 from one cell to the cell with EDC injection could be well controlled by adjusting the injection rate of EDC. As shown in Figure 3h, when the injection rate of EDC was increased from 0.01 mmol·h^{-1} (5.0×10^2 mM, 0.02 mL/h) to 0.02 mmol·h^{-1} (1.0×10^3 mM, 0.02 mL/h), we could observe that the delivery capacity will reach the maximum. Further increasing the EDC injection rate would not lead to a significant enhancement of the delivery capacity. This was probably due to the fact that, during the fast EDC injection, the diffusion of EDC from the right side cell to the left side cell was not negligible.

Selectivity of the Pumping Process. We also found that energy-driven loading process showed high selectivity. For instance, in the presence of another dye carrying positive charges (crystal violet, CV), AO7 could be loaded into the assemblies selectively (Figure 4). To demonstrate, we added EDC (4.8×10^{-5} mol, 2.0 equiv) into 3.0 mL of MES buffer solution (pH 5.5, 200 mM) containing $TMC_{10}COOH$ (2.4×10^{-5} mol, 8.0 mM), AO7 (1.1×10^{-7} mol, 0.038 mM), and CV (1.2×10^{-8} mol, 0.004 mM) and mixed them together. After keeping the reaction mixture at 25 °C for different periods of time, the mixture was filtered by using a 0.45 μm filter membrane to remove the assemblies. We found that the color of the obtained filtrate changed from Indian red to plum in the first 50 min and then turned back to Indian red in the next 540 min, probably due to different residual amounts of AO7 and CV in the solution (Figure 4a). By measuring the UV−vis spectra of the filtrates, we were able to determine the amounts of AO7 (Figure 4b) and CV (Figure 4c) in the filtrates and assemblies quantitatively over time. We found that the percentage of AO7 in the assemblies increased to 78% in 50 min and gradually decreased to 8% after 540 min (Figure 4b). At the same time, CV could be barely detected in the assemblies (Figure 4c). This means that AO7 was selectively

https://doi.org/10.1021/jacs.3c12228
J. Am. Chem. Soc. 2024, 146, 3323−3330

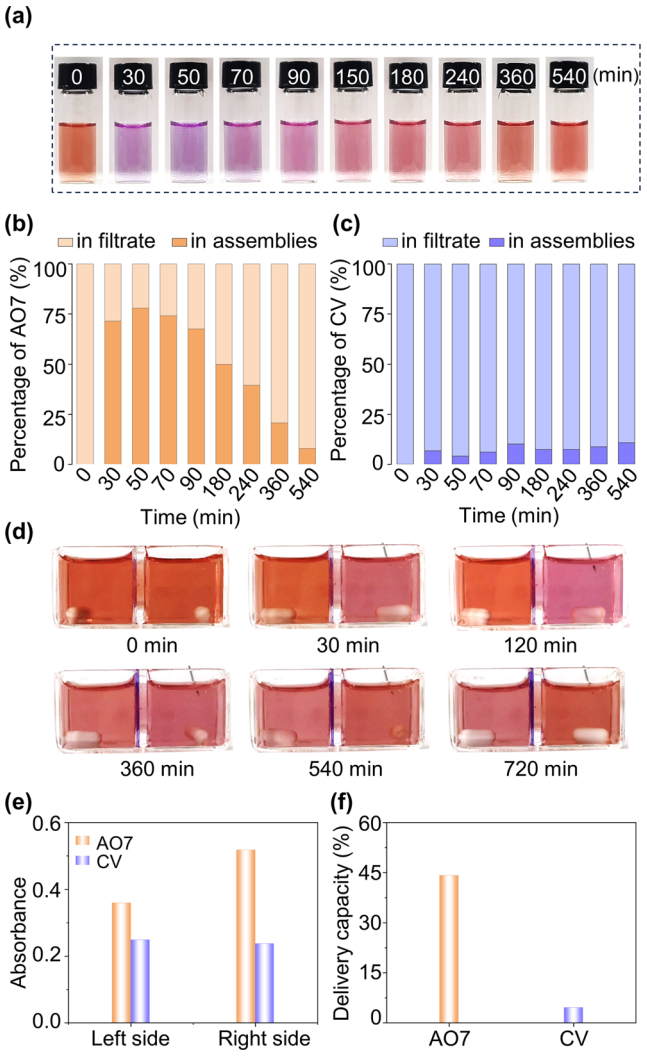

Figure 4. (a) Photographs of the filtrates at different periods after removing the assemblies through filtration. (b) Percentage of AO7 in the assemblies (dark color) and the filtrates (light color) against the time. (c) Percentage of CV in the assemblies (dark color) and the filtrate (light color) against the time. (d) Photographs of the two-cell container at different periods after the injection of EDC into the right side cell. (e) The histogram reports the absorbances of AO7 and CV at 720 min on the both sides cell. (f) Delivery capacity of AO7 and CV from the one side cell to another at 720 min.

loaded to the assemblies and released into the solution during the reaction between $TMC_{10}COOH$ and EDC, while CV remained in the solution all the time.

Subsequently, we were able to control the distribution of AO7 selectively, even in the presence of AO7 and CV by the consumption of chemical fuel EDC. As shown in Figure 4d, we utilized a two-cell container separated by a microporous membrane with a pore size of 0.45 μm again, filled with $TMC_{10}COOH$ (8.0 mM), AO7 (0.038 mM), and CV (0.004 mM) aqueous solution containing MES buffer (200 mM, pH 5.5). Then, EDC (2.0×10^3 mM) was continuously injected into the right side with a syringe at the rate of 0.04 mmol·h^{-1}. In the first 120 min, the color of the right cell became plum due to the free AO7 in solution being loaded into the assemblies. Then, the color of the left cell went lighter as well, caused by the diffusion of free AO7 from the left side to the right side cell. From 540 min, we could observe that the cell at the right side showed a darker color than the cell on the left side. The color difference between these two sides reached the maximum after 720 min of continually fueling the right side cell with EDC. After 720 min, from their UV−vis spectra, we were able to obtain the absorbance of AO7 on the left side at 0.36 and on the right side at 0.52 and the CV on the left side at 0.25 and on the right side at 0.24 (Figure 4e). By calculating the delivery capacity of these two small molecules, we found that the delivery capacity for AO7 was 44%, while for CV, the value was only 5%. These results clearly demonstrated that, using the continuous injection of EDC fuel, we were able to control the distribution of AO7 (Figure 4f) in a highly selective manner. To further refine this selectivity, we are actively pursuing strategies to discriminate between specific functional groups and tune binding affinities at a finer level.

CONCLUSIONS

In conclusion, by utilizing the reaction cycle between EDC and carboxylic acid, we were able to control the distribution of small molecules in the system at nonequilibrium states by actively pumping the small molecules even against the concentration gradient. Meanwhile, this transportation process shows high selectivity. We believe these achievements will contribute to the development of artificial active materials.

ASSOCIATED CONTENT

Supporting Information

The Supporting Information is available free of charge at https://pubs.acs.org/doi/10.1021/jacs.3c12228.

General information, materials, experimental procedures, compound characterization data, and kinetic model (PDF)

AUTHOR INFORMATION

Corresponding Authors

Jiajia Zhou − *South China Advanced Institute for Soft Matter Science and Technology, School of Emergent Soft Matter, Guangdong Provincial Key Laboratory of Functional and Intelligent Hybrid Materials and Devices, South China University of Technology, Guangzhou 510640, P. R. China;* orcid.org/0000-0002-2258-6757; Email: zhouj2@scut.edu.cn

Wei Zhang − *South China Advanced Institute for Soft Matter Science and Technology, School of Emergent Soft Matter, Guangdong Provincial Key Laboratory of Functional and Intelligent Hybrid Materials and Devices, South China University of Technology, Guangzhou 510640, P. R. China;* orcid.org/0000-0002-0658-7872; Email: weizhang@scut.edu.cn

Authors

Huimin Fu − *South China Advanced Institute for Soft Matter Science and Technology, School of Emergent Soft Matter, Guangdong Provincial Key Laboratory of Functional and Intelligent Hybrid Materials and Devices, South China University of Technology, Guangzhou 510640, P. R. China*

Nengjie Cao − *South China Advanced Institute for Soft Matter Science and Technology, School of Emergent Soft Matter, Guangdong Provincial Key Laboratory of Functional and Intelligent Hybrid Materials and Devices, South China University of Technology, Guangzhou 510640, P. R. China*

Wang Zeng − *National Centre for Inorganic Mass Spectrometry in Shanghai, Shanghai Institute of Ceramics, Chinese Academy of Sciences, Shanghai 200050, P. R. China*
Min Liao − *South China Advanced Institute for Soft Matter Science and Technology, School of Emergent Soft Matter, Guangdong Provincial Key Laboratory of Functional and Intelligent Hybrid Materials and Devices, South China University of Technology, Guangzhou 510640, P. R. China*
Shenglin Yao − *South China Advanced Institute for Soft Matter Science and Technology, School of Emergent Soft Matter, Guangdong Provincial Key Laboratory of Functional and Intelligent Hybrid Materials and Devices, South China University of Technology, Guangzhou 510640, P. R. China*

Complete contact information is available at: https://pubs.acs.org/10.1021/jacs.3c12228

Author Contributions

[§]H.F. and N.C. contributed equally to this work. All authors have given approval to the final version of the manuscript.

Notes

The authors declare no competing financial interest.

■ ACKNOWLEDGMENTS

This work is supported by the Natural Science Foundation (No. 21774037), the Guangdong Natural Science Foundation (No. 2018B030306039), the 111 Project (No. B18023), and the Recruitment Program of Guangdong (No. 2016ZT06C322).

■ REFERENCES

(1) (a) van Rossum, S. A. P.; Tena-Solsona, M.; van Esch, J. H.; Eelkema, R.; Boekhoven, J. Dissipative out-of-Equilibrium Assembly of Man-Made Supramolecular Materials. *Chem. Soc. Rev.* **2017**, *46*, 5519. (b) Bernheim-Groswasser, A.; Gov, N. S.; Safran, S. A.; Tzlil, S. Living Matter: Mesoscopic Active Materials. *Adv. Mater.* **2018**, *30*, No. 1707028. (c) Gentile, K.; Somasundar, A.; Bhide, A.; Sen, A. Chemically Powered Synthetic "Living" Systems. *Chem* **2020**, *6*, 2174. (d) Dong, Y.; Ramey-Ward, A. N.; Salaita, K. Programmable Mechanically Active Hydrogel-Based Materials. *Adv. Mater.* **2021**, *33*, No. 2006600.

(2) (a) Boekhoven, J.; Hendriksen, W. E.; Koper, G. J. M.; Eelkema, R.; van Esch, J. H. Transient Assembly of Active Materials Fueled by a Chemical Reaction. *Science* **2015**, *349*, 1075. (b) Merindol, R.; Walther, A. Materials Learning from Life: Concepts for Active, Adaptive and Autonomous Molecular Systems. *Chem. Soc. Rev.* **2017**, *46*, 5588. (c) Ashkenasy, G.; Hermans, T. M.; Otto, S.; Taylor, A. F. Systems Chemistry. *Chem. Soc. Rev.* **2017**, *46*, 2543. (d) te Brinke, E.; Groen, J.; Herrmann, A.; Heus, H. A.; Rivas, G.; Spruijt, E.; Huck, W. T. S. Dissipative Adaptation in Driven Self-Assembly Leading to Self-Dividing Fibrils. *Nat. Nanotechnol.* **2018**, *13*, 849. (e) Morrow, S. M.; Colomer, I.; Fletcher, S. P. A Chemically Fuelled Self-Replicator. *Nat. Commun.* **2019**, *10*, No. 1011. (f) Walther, A. Viewpoint: From Responsive to Adaptive and Interactive Materials and Materials Systems: A Roadmap. *Adv. Mater.* **2020**, *32*, No. 1905111. (g) Howlett, M. G.; Engwerda, A. H. J.; Scanes, R. J. H.; Fletcher, S. P. An Autonomously Oscillating Supramolecular Self-Replicator. *Nat. Chem.* **2022**, *14*, 805. (h) Singh, N.; Lopez-Acosta, A.; Formon, G. J. M.; Hermans, T. M. Chemically Fueled Self-Sorted Hydrogels. *J. Am. Chem. Soc.* **2022**, *144*, 410.

(3) (a) Soh, S.; Byrska, M.; Kandere-Grzybowska, K.; Grzybowski, B. A. Reaction-Diffusion Systems in Intracellular Molecular Transport and Control. *Angew. Chem., Int. Ed.* **2010**, *49*, 4170. (b) Lovrak, M.; Hendriksen, W. E. J.; Maity, C.; Mytnyk, S.; van Steijn, V.; Eelkema, R.; van Esch, J. H. Free-Standing Supramolecular Hydrogel Objects by Reaction-Diffusion. *Nat. Commun.* **2017**, *8*, No. 15317. (c) Chen, R.; Neri, S.; Prins, L. J. Enhanced Catalytic Activity under Non-Equilibrium Conditions. *Nat. Nanotechnol.* **2020**, *15*, 868. (d) Korevaar, P. A.; Kaplan, C. N.; Grinthal, A.; Rust, R. M.; Aizenberg, J. Non-Equilibrium Signal Integration in Hydrogels. *Nat. Commun.* **2020**, *11*, No. 386. (e) Fan, X.; Walther, A. Autonomous Transient pH Flips Shaped by Layered Compartmentalization of Antagonistic Enzymatic Reactions. *Angew. Chem., Int. Ed.* **2021**, *60*, 3619. (f) Maity, I.; Sharma, C.; Lossada, F.; Walther, A. Feedback and Communication in Active Hydrogel Spheres with pH Fronts: Facile Approaches to Grow Soft Hydrogel Structures. *Angew. Chem., Int. Ed.* **2021**, *60*, 22537. (g) Vyborna, Y.; Galas, J.-C.; Estevez-Torres, A. DNA-Controlled Spatiotemporal Patterning of a Cytoskeletal Active Gel. *J. Am. Chem. Soc.* **2021**, *143*, 20022. (h) Zhang, R.; Redford, S. A.; Ruijgrok, P. V.; Kumar, N.; Mozaffari, A.; Zemsky, S.; Dinner, A. R.; Vitelli, V.; Bryant, Z.; Gardel, M. L.; de Pablo, J. J. Spatiotemporal Control of Liquid Crystal Structure and Dynamics through Activity Patterning. *Nat. Mater.* **2021**, *20*, 875. (i) Selmani, S.; Schwartz, E.; Mulvey, J. T.; Wei, H.; Grosvirt-Dramen, A.; Gibson, W.; Hochbaum, A. I.; Patterson, J. P.; Ragan, R.; Guan, Z. Electrically Fueled Active Supramolecular Materials. *J. Am. Chem. Soc.* **2022**, *144*, 7844. (j) Bai, S.; Wang, H.; Gu, G.; Gou, Y.; Zhou, X.; Yu, S.; Wang, Q.; Guo, X.; Wang, Y. Transient and Directional Growth of Supramolecular Hydrogels through Reaction−Diffusion-Mediated Self-Assembly for Dynamic Wet Gluing. *Chem. Eng. J.* **2023**, *475*, No. 146125.

(4) (a) Chen, R.; Das, K.; Cardona, M. A.; Gabrielli, L.; Prins, L. J. Progressive Local Accumulation of Self-Assembled Nanoreactors in a Hydrogel Matrix through Repetitive Injections of ATP. *J. Am. Chem. Soc.* **2022**, *144*, 2010. (b) Cao, Y.; Gabrielli, L.; Frezzato, D.; Prins, L. J. Persistent ATP-Concentration Gradients in a Hydrogel Sustained by Chemical Fuel Consumption. *Angew. Chem., Int. Ed.* **2023**, *62*, No. e202215421.

(5) (a) Gouaux, E.; MacKinnon, R. Principles of Selective Ion Transport in Channels and Pumps. *Science* **2005**, *310*, 1461. (b) Castillo, J. P.; Rui, H.; Basilio, D.; Das, A.; Roux, B.; Latorre, R.; Bezanilla, F.; Holmgren, M. Mechanism of Potassium Ion Uptake by the Na^+/K^+-ATPase. *Nat. Commun.* **2015**, *6*, No. 7622.

(6) (a) Tena-Solsona, M.; Rieß, B.; Grötsch, R. K.; Löhrer, F. C.; Wanzke, C.; Käsdorf, B.; Bausch, A. R.; Müller-Buschbaum, P.; Lieleg, O.; Boekhoven, J. Non-Equilibrium Dissipative Supramolecular Materials with a Tunable Lifetime. *Nat. Commun.* **2017**, *8*, No. 15895. (b) Tena-Solsona, M.; Wanzke, C.; Riess, B.; Bausch, A. R.; Boekhoven, J. Self-Selection of Dissipative Assemblies Driven by Primitive Chemical Reaction Networks. *Nat. Commun.* **2018**, *9*, No. 2044. (c) Kriebisch, B. A. K.; Jussupow, A.; Bergmann, A. M.; Kohler, F.; Dietz, H.; Kaila, V. R. I.; Boekhoven, J. Reciprocal Coupling in Chemically Fueled Assembly: A Reaction Cycle Regulates Self-Assembly and Vice Versa. *J. Am. Chem. Soc.* **2020**, *142*, 20837. (d) Wanzke, C.; Tena-Solsona, M.; Rieß, B.; Tebcharani, L.; Boekhoven, J. Active Droplets in a Hydrogel Release Drugs with a Constant and Tunable Rate. *Mater. Horiz.* **2020**, *7*, 1397. (e) Späth, F.; Donau, C.; Bergmann, A. M.; Kränzlein, M.; Synatschke, C. V.; Rieger, B.; Boekhoven, J. Molecular Design of Chemically Fueled Peptide−Polyelectrolyte Coacervate-Based Assemblies. *J. Am. Chem. Soc.* **2021**, *143*, 4782. (f) Kriebisch, C. M. E.; Bergmann, A. M.; Boekhoven, J. Fuel-Driven Dynamic Combinatorial Libraries. *J. Am. Chem. Soc.* **2021**, *143*, 7719. (g) Schnitter, F.; Bergmann, A. M.; Winkeljann, B.; Rodon Fores, J.; Lieleg, O.; Boekhoven, J. Synthesis and Characterization of Chemically Fueled Supramolecular Materials Driven by Carbodiimide-Based Fuels. *Nat. Protoc.* **2021**, *16*, 3901. (h) Donau, C.; Späth, F.; Stasi, M.; Bergmann, A. M.; Boekhoven, J. Phase Transitions in Chemically Fueled, Multiphase Complex Coacervate Droplets. *Angew. Chem., Int. Ed.* **2022**, *61*, No. e202211905. (i) Stasi, M.; Monferrer, A.; Babl, L.; Wunnava, S.; Dirscherl, C. F.; Braun, D.; Schwille, P.; Dietz, H.; Boekhoven, J. Regulating DNA-Hybridization Using a Chemically Fueled Reaction Cycle. *J. Am. Chem. Soc.* **2022**, *144*, 21939. (j) Späth, F.; Maier, A. S.; Stasi, M.; Bergmann, A. M.; Halama, K.; Wenisch, M.; Rieger, B.; Boekhoven, J. The Role of Chemically Innocent Polyanions in Active, Chemically Fueled Complex Coacervate Droplets. *Angew. Chem., Int.*

Ed. **2023**, *62*, No. e202309318. (k) Bergmann, A. M.; Bauermann, J.; Bartolucci, G.; Donau, C.; Stasi, M.; Holtmann Spötter, A.-L.; Jülicher, F.; Weber, C. A.; Boekhoven, J. Liquid Spherical Shells Non-Equilibrium Steady State of Active Droplets. *Nat. Commun.* **2023**, *14*, No. 6552.

(7) (a) Kariyawasam, L. S.; Hartley, C. S. Dissipative Assembly of Aqueous Carboxylic Acid Anhydrides Fueled by Carbodiimides. *J. Am. Chem. Soc.* **2017**, *139*, 11949. (b) Zhang, B.; Jayalath, I. M.; Ke, J.; Sparks, J. L.; Hartley, C. S.; Konkolewicz, D. Chemically Fueled Covalent Crosslinking of Polymer Materials. *Chem. Commun.* **2019**, *55*, 2086. (c) Kariyawasam, L. S.; Kron, J. C.; Jiang, R.; Sommer, A. J.; Hartley, C. S. Structure−Property Effects in the Generation of Transient Aqueous Benzoic Acid Anhydrides by Carbodiimide Fuels. *J. Org. Chem.* **2020**, *85*, 682. (d) Hossain, M. M.; Atkinson, J. L.; Hartley, C. S. Dissipative Assembly of Macrocycles Comprising Multiple Transient Bonds. *Angew. Chem., Int. Ed.* **2020**, *59*, 13807. (e) Jayalath, I. M.; Wang, H.; Mantel, G.; Kariyawasam, L. S.; Hartley, C. S. Chemically Fueled Transient Geometry Changes in Diphenic Acids. *Org. Lett.* **2020**, *22*, 7567. (f) Dodo, O. J.; Petit, L.; Rajawasam, C. W. H.; Hartley, C. S.; Konkolewicz, D. Tailoring Lifetimes and Properties of Carbodiimide-Fueled Covalently Cross-Linked Polymer Networks. *Macromolecules* **2021**, *54*, 9860. (g) Hossain, M. M.; Jayalath, I. M.; Baral, R.; Hartley, C. S. Carbodiimide-Induced Formation of Transient Polyether Cages**. *ChemSystemsChem.* **2022**, *4*, No. e202200016. (h) Rajawasam, C. W. H.; Tran, C.; Weeks, M.; McCoy, K. S.; Ross-Shannon, R.; Dodo, O. J.; Sparks, J. L.; Hartley, C. S.; Konkolewicz, D. Chemically Fueled Reinforcement of Polymer Hydrogels. *J. Am. Chem. Soc.* **2023**, *145*, 5553.

(8) (a) Cheng, M.; Qian, C.; Ding, Y.; Chen, Y.; Xiao, T.; Lu, X.; Jiang, J.; Wang, L. Writable and Self-Erasable Hydrogel Based on Dissipative Assembly Process from Multiple Carboxyl Tetraphenylethylene Derivative. *ACS Mater. Lett.* **2020**, *2*, 425. (b) Panja, S.; Dietrich, B.; Adams, D. J. Chemically Fuelled Self-Regulating Gel-to-Gel Transition. *ChemSystemsChem.* **2020**, *2*, No. e1900038. (c) Heckel, J.; Loescher, S.; Mathers, R. T.; Walther, A. Chemically Fueled Volume Phase Transition of Polyacid Microgels. *Angew. Chem., Int. Ed.* **2021**, *60*, 7117. (d) Bai, S.; Niu, X.; Wang, H.; Wei, L.; Liu, L.; Liu, X.; Eelkema, R.; Guo, X.; van Esch, J. H.; Wang, Y. Chemical Reaction Powered Transient Polymer Hydrogels for Controlled Formation and Free Release of Pharmaceutical Crystals. *Chem. Eng. J.* **2021**, *414*, No. 128877. (e) Xu, H.; Bai, S.; Gu, G.; Gao, Y.; Sun, X.; Guo, X.; Xuan, F.; Wang, Y. Bioinspired Self-Resettable Hydrogel Actuators Powered by a Chemical Fuel. *ACS Appl. Mater. Interfaces* **2022**, *14*, 43825.

(9) (a) Garcia, M. E. D.; Sanz-Medel, A. Dye-Surfactant Interactions: A Review. *Talanta* **1986**, *33*, 255. (b) Fazeli, S.; Sohrabi, B.; Tehrani-Bagha, A. R. The Study of Sunset Yellow Anionic Dye Interaction with Gemini and Conventional Cationic Surfactants in Aqueous Solution. *Dyes Pigm.* **2012**, *95*, 768.

(10) (a) Kretschmer, M.; Winkeljann, B.; Kriebisch, B. A. K.; Boekhoven, J.; Lieleg, O. Viscoelastic Behavior of Chemically Fueled Supramolecular Hydrogels under Load and Influence of Reaction Side Products. *Commun. Mater.* **2021**, *2*, No. 97. (b) Zeng, W.; Fan, C.; Xing, X.; Cheng, H.; Fu, H.; Ma, B.; Yang, Z.; Zhang, R.; Zhang, W. Out of Equilibrium Coil-Helix Transition Driven by Chemical Fuels. *Giant* **2021**, *7*, No. 100067.

https://doi.org/10.1021/jacs.3c12228
J. Am. Chem. Soc. 2024, 146, 3323−3330

Supporting Information for

Pumping Small Molecules Selectively through an Energy-Assisted Assembling Process at Nonequilibrium States

Huimin Fu,[a,§] Nengjie Cao,[a,§] Wang Zeng,[b] Min Liao,[a] Shenglin Yao,[a] Jiajia Zhou,[a,*] Wei Zhang[a,*]

[a]South China Advanced Institute for Soft Matter Science and Technology, School of Emergent Soft Matter, Guangdong Provincial Key Laboratory of Functional and Intelligent Hybrid Materials and Devices, South China University of Technology, Guangzhou 510640, P. R. China

[b]National Centre for Inorganic Mass Spectrometry in Shanghai, Shanghai Institute of Ceramics, Chinese Academy of Sciences, Shanghai 200050, P. R. China

[*]Email: zhouj2@scut.edu.cn; weizhang@scut.edu.cn

Table of Contents

1. General

Unless otherwise noted, ^{1}H NMR spectra were recorded at 25 ℃ using a JEOL model JNM-ECZ500R spectrometer, operating at 500 MHz, where chemical shifts (δ in ppm) were determined with respect to non-deuterated solvent residues as internal references. Ultraviolet−visible (UV−vis) absorption spectra were recorded on the SHIMADZU model UV-3600 Plus UV−vis spectrophotometer using a quartz cell with 10 mm optical path length. Dynamic light scattering (DLS) was conducted on a Brookhaven model Omni particle size tester using a cell with 10 mm optical path length. Bright-field micrographs were recorded using Zeiss model LSM 880 NLO confocal laser scanning microscope using a 63x oil immersion objective. Atomic force microscope (AFM) images were recorded using an Oxford Instruments Asylum Research model Cypher VRS AFM microscope with Olympus AC200TS-R3 probe for gas phase scanning. Transmission electron microscope (TEM) images were recorded on a JEOL model JEM−1400 electron microscope operating at 120 kV, each of the samples was deposited on a specimen Cu grid covered with carbon support films manufactured by Zhongjingkeyi Technology Co., Ltd. Scanning electron microscope (SEM) images were recorded on a JEOL model JSM−7900F SEM microscope operating at 5 kV. Each of the samples was deposited on a silicon substrate followed by sputtering with Pt. The pH was recorded using the pH meter (Leizi, PHS−2F).

2. Materials

Unless otherwise noted, all commercial chemicals and reagents were obtained from commercial sources and used as received without further purification. 11-Bromoundecanoic acid, trimethylamine (30% in ethanol, TMA), acid orange (AO7), crystal violet (CV), 1-ethyl-3-(3-(dimethylamino)propyl) carbodiimide hydrochloride (EDC·HCl), 2-(N-morpholino)ethanesulfonic acid (MES) buffer, sodium hydroxide (NaOH), deuterium oxide (D_2O), deuterated dimethyl sulfoxide (DMSO-d_6), ethanol (EtOH) were purchased from Adamas chemicals. Ethyl ether was purchased from Guangzhou Chemical Reagent Factory and the deionized water used in all experiments came from our laboratory.

3. Experimental Procedures

1. Precursor synthesis and purification

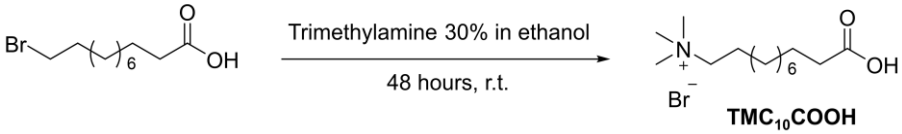

Scheme S1. Synthesis of the quaternary ammonium-acid $TMC_{10}COOH$

Compound $TMC_{10}COOH$ was prepared according to the reported procedure.[1] 11-bromoundecanoic acid (8.00 g, 0.03 mol) was mixed with trimethylamine (30% in ethanol, TMA) (70 mL) and stirred for 48 h at room temperature. Then, the solvent was removed by vacuum

evaporation, the obtained solid residue was recrystallized from methanol/ethyl ether (1:1.5, v/v) to afford a white powder as $TMC_{10}COOH$ (3.75 g, yield 51%). ^{1}H NMR (500 MHz, DMSO-d_6) δ (ppm) 11.96 (s, 1H), 3.28 (t, J = 5.0 Hz, 2H), 3.05 (s, 9H), 2.19 (t, J = 7.0 Hz, 2H), 1.71 – 1.62 (m, 2H), 1.53 – 1.44 (m, 2H), 1.34 – 1.22 (m, 12H).

2. Fabrication of the samples of AFM, SEM and TEM

We added EDC (1.6×10^{-5} mol, 2.0 equiv.) into 1.0 mL MES buffer solution (pH 5.5, 200 mM) containing $TMC_{10}COOH$ (8.0×10^{-6} mol, 8.0 mM) and AO7 (3.8×10^{-8} mol, 0.038 mM) and mixed together. After keeping the reaction mixture at 25 °C for 10 min, the mixture was centrifuged to remove the supernatant first, and then transferred the remaining solid to silicon substrate and Cu grid.

3. Preparation of polyacrylamide hydrogel

The polyacrylamide (PAM) hydrogel was prepared by the free radical polymerization of an aqueous solution containing acrylamide (AM, 1.4×10^3 mM), N, N´-methylenebisacrylamide (Bis, 6.5 mM) and 2-hydroxy-4'-(2-hydroxyethoxy)-2-methyl-propiophe (Irgacure2959, 8.9 mM) under UV irradiation (3.0 mW, 4.0 h). Then, the hydrogel sample was soaked with the MES buffer solution (pH 5.5, 200 mM) containing $TMC_{10}COOH$ (8.0 mM) and AO7 (0.038 mM) for 48.0 h.

4. Analysis of the fuel-driven reaction cycle by in situ ^{1}H NMR

The kinetics of the chemical reaction network were monitored over time using in situ ^{1}H NMR spectroscopy. The spectra were used to determine the concentrations of precursor, activated anhydride, fuel (1-ethyl-3-(3-(dimethylamino)propyl) carbodiimide hydrochloride, EDC) and waste (1-[3-(dimethylamine)propyl]-3-ethylurea, EDU) in solution over time. In this experiment, EDC (2.0×10^{-5} mol, 2.0 equiv.) was added into 0.5 mL D_2O solution containing $TMC_{10}COOH$ (1.0×10^{-5} mol, 20.0 mM), 1,4-dioxane (50.0 mM, as an internal standard) and MES buffer (pD = 5.5, 200 mM). By comparing the integral area between peak intensity with chemical shift of the precursor at 2.32 ppm (–CH_2COOH, t), anhydride at 2.59 ppm (–CH_2CO, t), EDC at 1.19 ppm (–CH_3, t) and EDU at 1.12 ppm (–CH_3, t) to the integral area of the internal standard with a chemical shift at 3.78 ppm to determine the concentrations of corresponding compounds.

5. Small molecules pumping experiment.

The experiment was carried out using a two-cell container separated by a microporous membrane with a pore size of 0.45 μm microporous membrane. The length, width, and height of the cells were 20 mm. The cross-sectional area between the two cells was 1.3×10^3 mm^2. 20 mL of MES buffer solution containing $TMC_{10}COOH$ (8.0 mM) and AO7 (0.038 mM) was prepared

freshly. 6.0 mL of sample was added to the left side cell and 6.5 mL was added to the right side cell, then stirred at 260 rpm with a 4 mm × 10 mm stir bar using a stirrer (SUNNE®, SN-MS-3D). Meanwhile, A syringe pump was used to supply a continuous flow of the fuel EDC with injection rate at 0.01 mmol·h^{-1}, 0.02 mmol·h^{-1}, 0.04 mmol·h^{-1}, and 0.06 mmol·h^{-1} to the right side cell, respectively.

4. Kinetic Model

The kinetic model was used to predict the evolution of compounds involved in the chemical reaction network over time.[2] The model was described in detail below. The rate constants we used in this work were given in Tables S2 and S3.

1. Description of the kinetic model

A kinetic model was written in Python that described each reaction involved in the chemical reaction network. The model was used to fit the obtained ^{1}H NMR data that described the evolution of the concentrations of precursor ($TMC_{10}COOH$), product $(TMC_{10}CO)_2O$), fuel (EDC), and waste (EDU) over time.

The system was analyzed using the following model:

$$E \xrightarrow{k_0} U \tag{1}$$

$$Ac + E \xrightarrow{k_1} I \tag{2}$$

$$I + Ac \xrightarrow{k_i^{An}} An + U \tag{3}$$

$$I \xrightarrow{k_i^{Ac}} Ac + U \tag{4}$$

$$An \xrightarrow{k_2} 2Ac \tag{5}$$

where Ac is the $TMC_{10}COOH$, E is the EDC, I is an activated carboxylic acid intermediate, An is the $(TMC_{10}CO)_2O$, and U is the EDU. Reaction (1) corresponds to the direct hydrolysis of EDC to EDU. Reaction (2) shows the activation reaction of the precursor with EDC to form the intermediate molecule. Reaction (3) is the intramolecular anhydride formation reaction. Reaction (4) depicts the direct hydrolysis of the intermediate molecule. Reaction (5) shows the hydrolysis of the anhydride to the initial precursor.

The mechanism translates into the following set of differential equations:

$$\frac{d[\mathrm{Ac}]}{dt} = -k_1[\mathrm{E}][\mathrm{Ac}] - k_i^{An}[\mathrm{I}][\mathrm{Ac}] + k_i^{Ac}[\mathrm{I}] + 2k_2[\mathrm{An}] \quad (6)$$

$$\frac{d[\mathrm{An}]}{dt} = +k_i^{An}[\mathrm{I}][\mathrm{Ac}] - k_2[\mathrm{An}] \quad (7)$$

$$\frac{d[\mathrm{I}]}{dt} = +k_1[\mathrm{E}][\mathrm{Ac}] - k_i^{An}[\mathrm{I}][\mathrm{Ac}] - k_i^{Ac}[\mathrm{I}] \quad (8)$$

$$\frac{d[\mathrm{E}]}{dt} = -k_1[\mathrm{E}][\mathrm{Ac}] - k_0[\mathrm{E}] \quad (9)$$

$$\frac{d[\mathrm{U}]}{dt} = +k_i^{Ac}[\mathrm{I}] + k_i^{An}[\mathrm{I}][\mathrm{Ac}] + k_0[\mathrm{E}] \quad (10)$$

If we assume a steady-state in [I], we obtain instead:

$$\frac{d[\mathrm{Ac}]}{dt} = -k_1[\mathrm{E}][\mathrm{Ac}] + 2k_2[\mathrm{An}] + \frac{k_1 K[\mathrm{E}][\mathrm{Ac}]}{K + [\mathrm{Ac}]} - \frac{k_1[\mathrm{E}][\mathrm{Ac}]^2}{K + [\mathrm{Ac}]} \quad (11)$$

$$\frac{d[\mathrm{An}]}{dt} = + \frac{k_1[\mathrm{E}][\mathrm{Ac}]^2}{K + [\mathrm{Ac}]} - k_2[\mathrm{An}] \quad (12)$$

$$\frac{d[\mathrm{E}]}{dt} = -k_1[\mathrm{E}][\mathrm{Ac}] - k_0[\mathrm{E}] \quad (13)$$

$$\frac{d[\mathrm{U}]}{dt} = +k_1[\mathrm{E}][\mathrm{Ac}] + k_0[\mathrm{E}] \quad (14)$$

Where $K = k_i^{Ac} / k_i^{An}$ (i.e., direct hydrolysis of the intermediate vs anhydride formation). The k and K are explicitly fit as parameters, as are the initial concentrations of EDC ($[\mathrm{E}]_0$) and acid ($[\mathrm{Ac}]_0$). The other starting concentrations ($[\mathrm{An}]_0$, $[\mathrm{I}]_0$, $[\mathrm{U}]_0$) are assumed to be 0. The yield of anhydride can be calculated by:

$$\text{Yield} = \frac{[\mathrm{An}]}{0.5[\mathrm{Ac}]_0} \quad (15)$$

2. Kinetic diffused phase separation system model

A kinetic diffused phase separation system model was written in Python that described the evolution of the concentrations of $TMC_{10}COOH$, $(TMC_{10}CO)_2O$, EDC, and EDU over time in both sides cell. In this experiment, the chemical fuel EDC was continuously injected into the right side cell.

$$\frac{d[\mathrm{Ac}_l]}{dt} = -\frac{DS([\mathrm{Ac}_l] - [\mathrm{Ac}_r])}{V_l x} \tag{16}$$

$$\frac{d[\mathrm{Ac}_r]}{dt} = -k_1[\mathrm{E}][\mathrm{Ac}_r] + 2k_2([\mathrm{An}^{(p)}] + [\mathrm{An}^{(r)}]) + \frac{k_1 K[\mathrm{E}][\mathrm{Ac}_r]}{K + [\mathrm{Ac}_r]} - \frac{k_1[\mathrm{E}][\mathrm{Ac}_r]^2}{K + [\mathrm{Ac}_r]} + \frac{DS([\mathrm{Ac}_l] - [\mathrm{Ac}_r])}{V_r x} \tag{17}$$

$$\frac{d[\mathrm{E}]}{dt} = -k_1[\mathrm{E}][\mathrm{Ac}_r] - k_0[\mathrm{E}] + v \tag{18}$$

$$\frac{d[\mathrm{U}]}{dt} = +k_1[\mathrm{E}][\mathrm{Ac}_r] + k_0[\mathrm{E}] \tag{19}$$

$$\frac{d[\mathrm{An}^{(p)}]}{dt} = \begin{cases} 0 & , \quad [\mathrm{An}^{(p)}] \geq [\mathrm{An}_{eq}^{(p)}] \\ \dfrac{k_1[\mathrm{E}][\mathrm{Ac}_r]^2}{K + [\mathrm{Ac}_r]} - k_2[\mathrm{An}^{(p)}], & [\mathrm{An}^{(p)}] < [\mathrm{An}_{eq}^{(p)}] \end{cases} \tag{20}$$

$$\frac{d[\mathrm{An}^{(r)}]}{dt} = \begin{cases} \dfrac{k_1[\mathrm{E}][\mathrm{Ac}_r]^2}{K + [\mathrm{Ac}_r]} - k_2([\mathrm{An}^{(r)}] + [\mathrm{An}^{(p)}]), & [\mathrm{An}^{(p)}] \geq [\mathrm{An}_{eq}^{(p)}] \\ 0 & , \quad [\mathrm{An}^{(p)}] < [\mathrm{An}_{eq}^{(p)}] \end{cases} \tag{21}$$

Where Ac_r is the precursor of the right side cell, Ac_l is the precursor of the left side cell, $\mathrm{An}^{(p)}$ is the anhydride in solution in free state, $\mathrm{An}^{(r)}$ is the anhydride in assemblies, $\mathrm{An}_{eq}^{(p)}$ is the critical concentration of $(\mathrm{TMC}_{10}\mathrm{CO})_2\mathrm{O}$ when the coassemblies start to form, E is the EDC, v is the injection rate, D is diffusion coefficient, S is diffusion area, x is the thickness of membrane. V_r is the volume of the solution in the right side cell, V_l is the volume of the solution in the left side cell. To simplify the theoretical model, we assumed that the anhydride production on the right side cell could not diffuse to the left in the whole process.

5. Supporting Figures and Tables

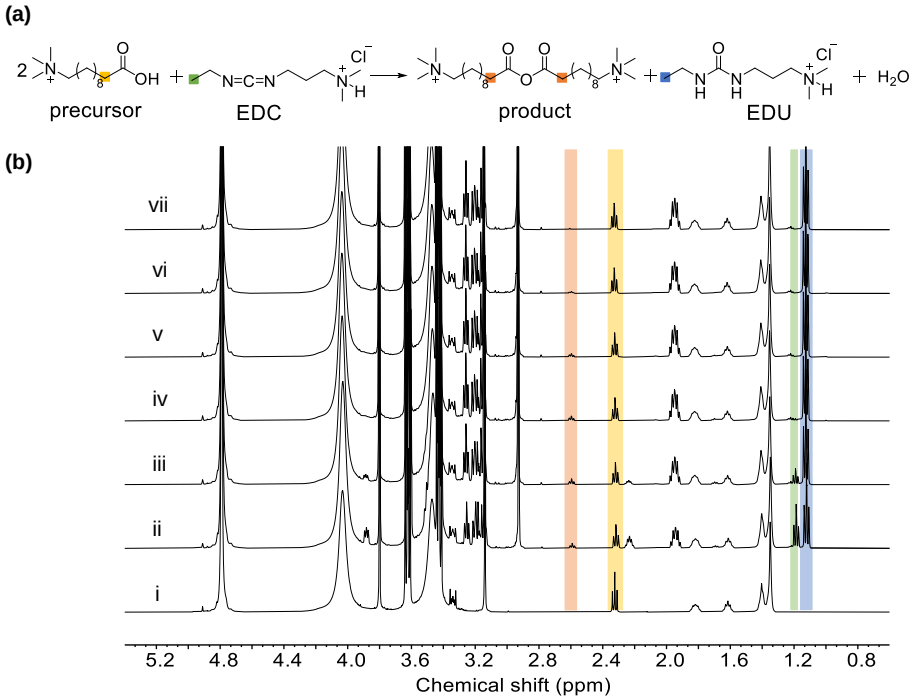

Figure S1. (a) The reaction route. (b) Time-dependent ^{1}H NMR spectra of precursor (20 mM) fueled with EDC (40 mM, 2.0 equiv.) in MES buffer solution (pD 5.5, 200 mM). The highlighted regions represent the protons related to compounds shown in Figure S1a: yellow (precursor), orange (product), green (EDC), and blue (EDU). (i) 0 min; (ii) 10 min; (iii) 20 min; (iv) 40 min; (v) 60 min; (vi) 100 min; (vii) 160 min.

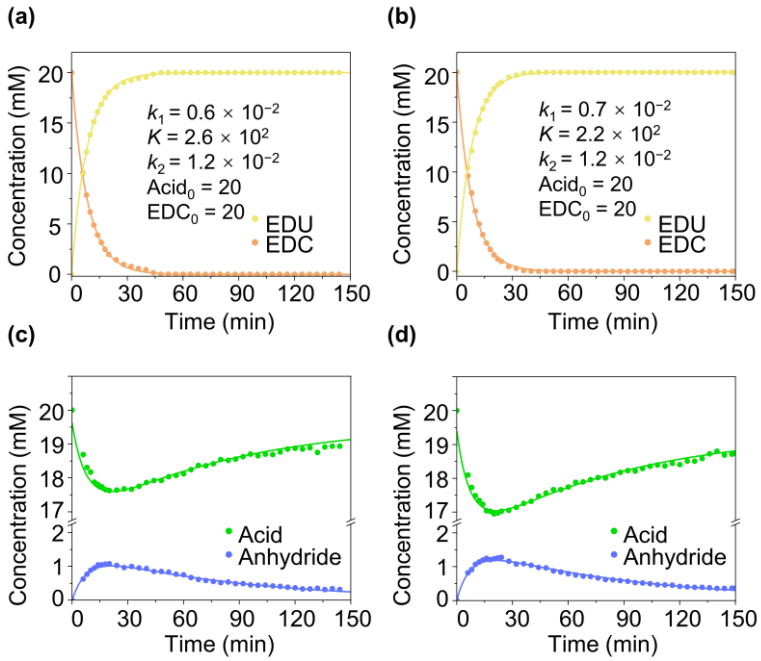

Figure S2. Kinetic traces of $TMC_{10}COOH$ (20 mM) with EDC (20 mM, 1.0 equiv.). The dots represent the data obtained by ^{1}H NMR. The solid lines represent the calculated data using the kinetic model.

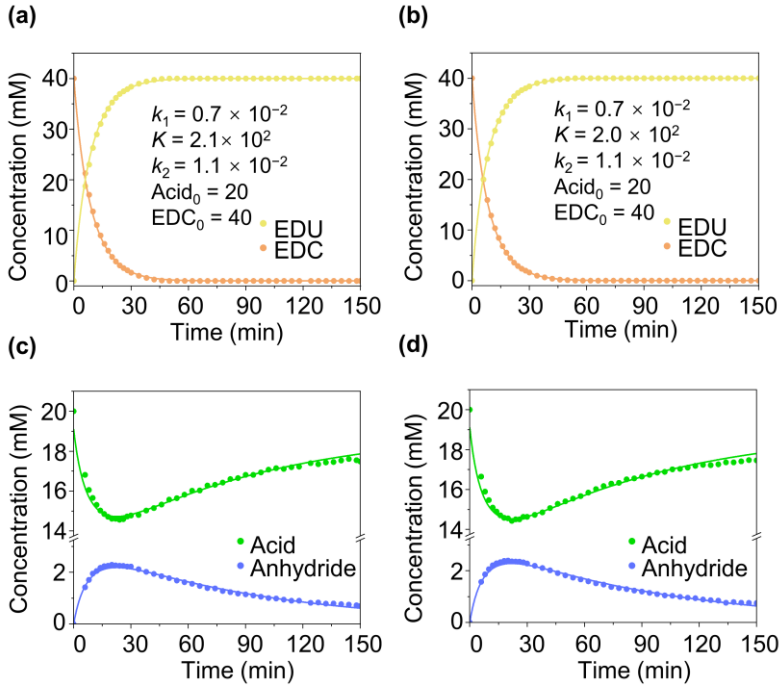

Figure S3. Kinetic traces of $TMC_{10}COOH$ (20 mM) with EDC (40 mM, 2.0 equiv.). The dots represent the data obtained by ^{1}H NMR. The solid lines represent the calculated data using the kinetic model.

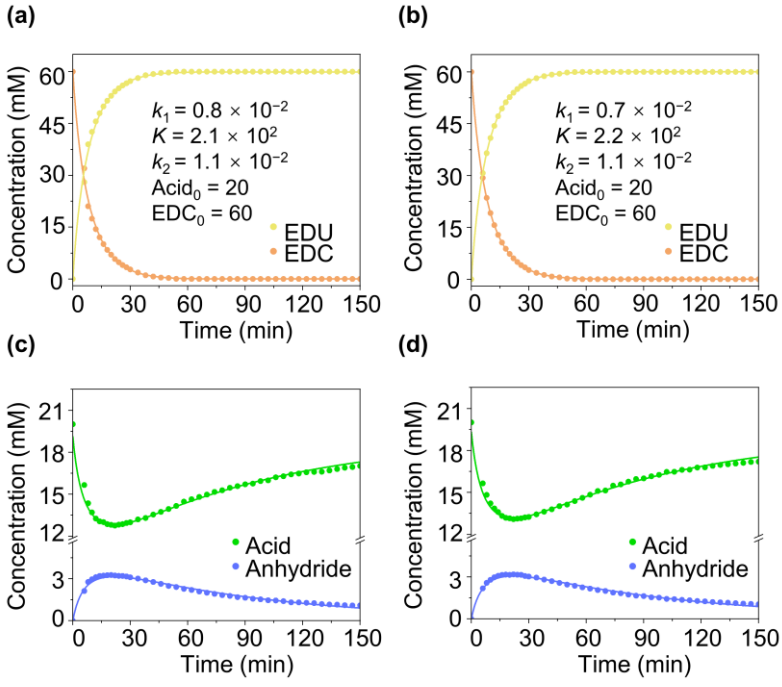

Figure S4. Kinetic traces of $TMC_{10}COOH$ (20 mM) with EDC (60 mM, 3.0 equiv.). The dots represent the data obtained by ^{1}H NMR. The solid lines represent the calculated data using the kinetic model.

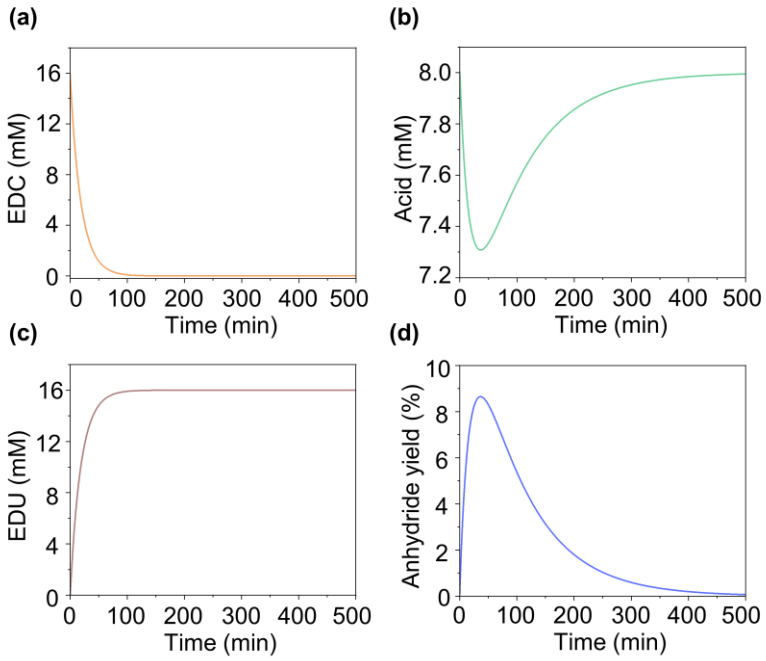

Figure S5. Simulated behaviors of the precursor (8.0 mM) system with EDC addition at a frequency of once (16.0 mM*1). (a) EDC concentration vs time, (b) precursor concentration vs time, (c) EDU concentration vs time and (d) anhydride yield vs time.

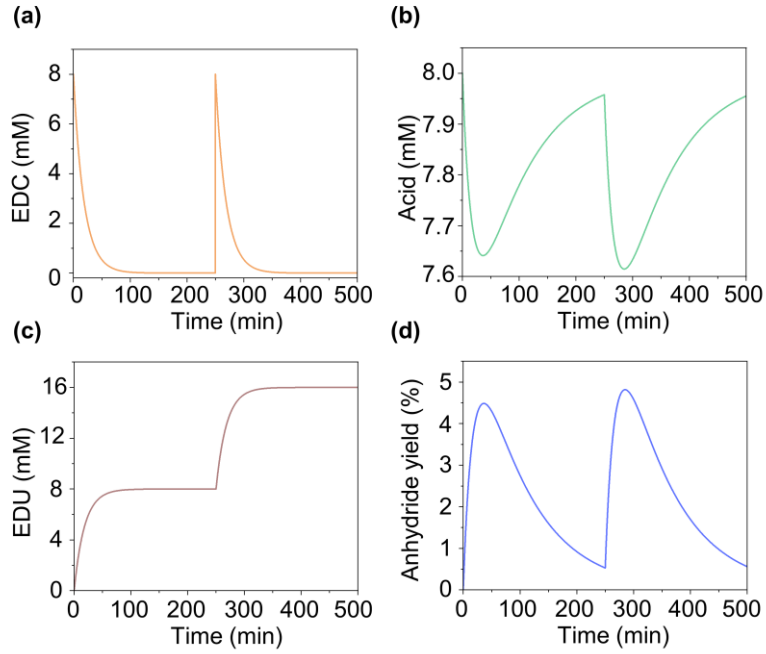

Figure S6. Simulated behaviors of the precursor (8.0 mM) system with EDC addition at a frequency of twice (8.0 mM*2). (a) EDC concentration vs time, (b) precursor concentration vs time, (c) EDU concentration vs time and (d) anhydride yield vs time.

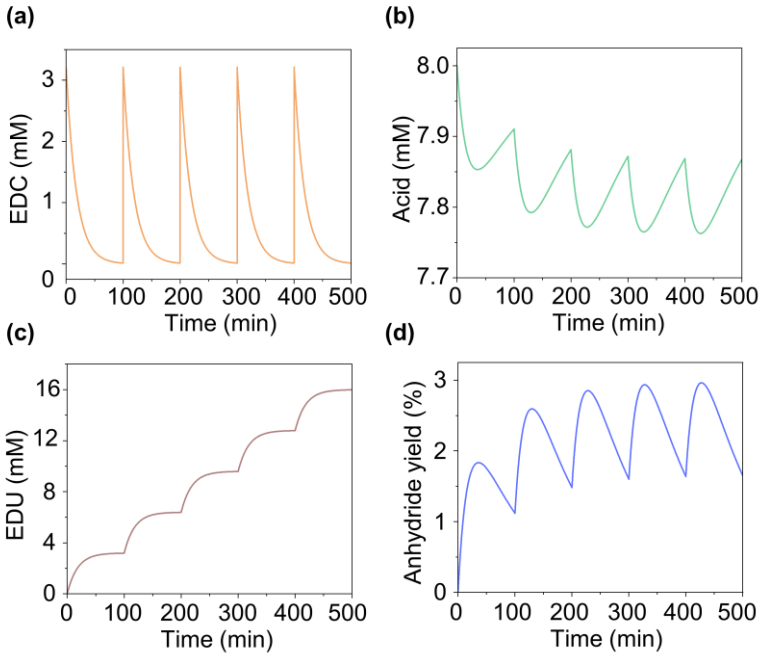

Figure S7. Simulated behaviors of the precursor (8.0 mM) system with EDC addition at a frequency of five times (3.2 mM*5). (a) EDC concentration vs time, (b) precursor concentration vs time, (c) EDU concentration vs time and (d) anhydride yield vs time.

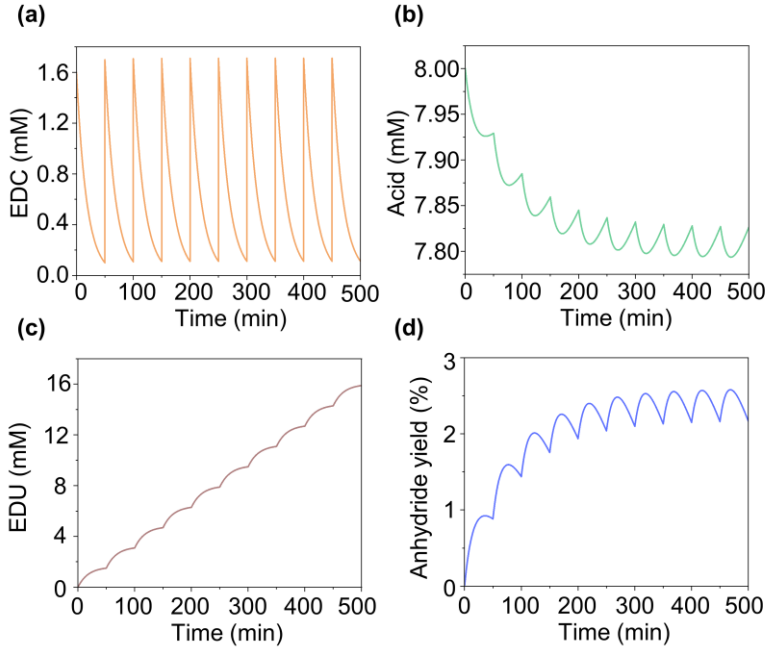

Figure S8. Simulated behaviors of the precursor (8.0 mM) system with EDC addition at a frequency of ten times (1.6 mM*10). (a) EDC concentration vs time, (b) precursor concentration vs time, (c) EDU concentration vs time and (d) anhydride yield vs time.

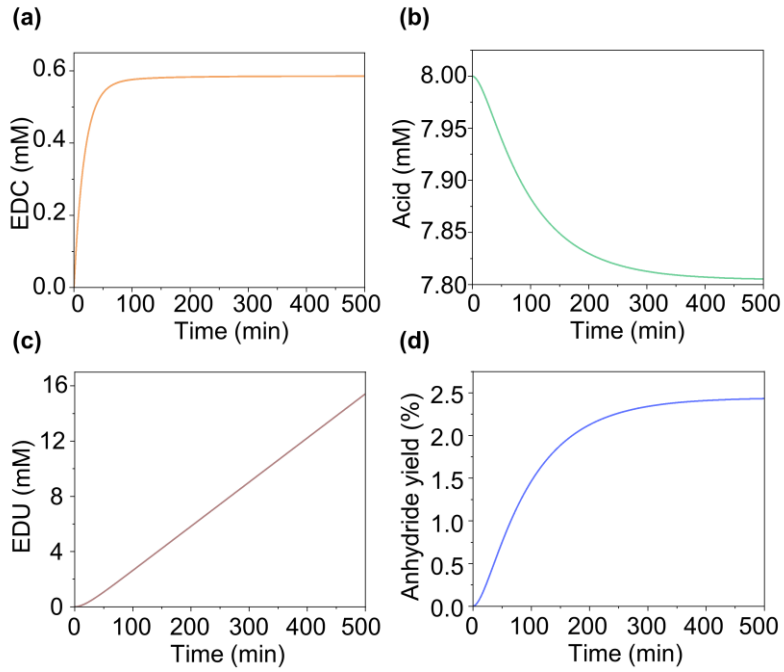

Figure S9. Simulated behaviors of the precursor (8.0 mM) system with EDC addition in a continuous manner. (a) EDC concentration vs time, (b) precursor concentration vs time, (c) EDU concentration vs time and (d) anhydride yield vs time.

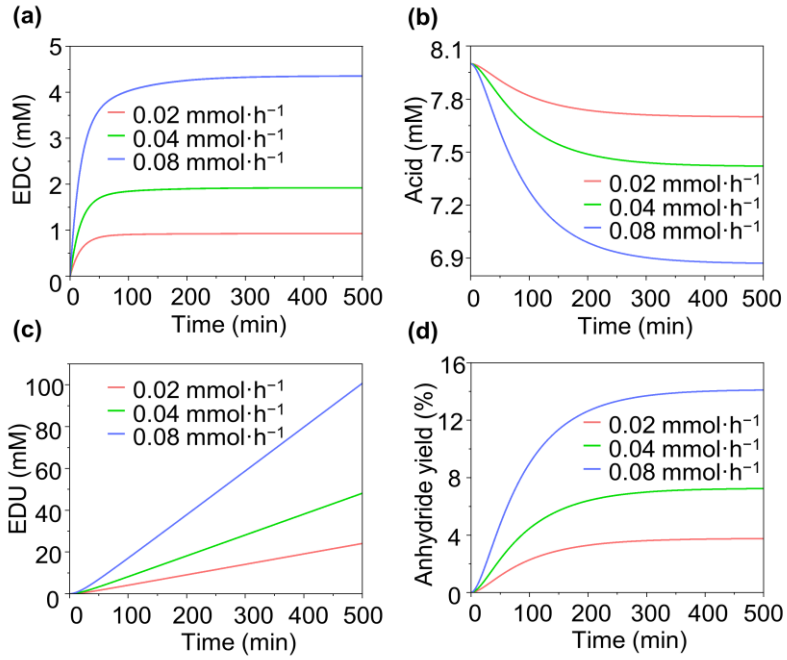

Figure S10. Simulated behaviors of the 8.0 mM precursor in 6.5 mL solution with EDC at an injection rate of 0.02 mmol·h^{-1} (red curve), 0.04 mmol·h^{-1} (green curve) and 0.08 mmol·h^{-1} (blue curve), respectively. (a) EDC concentration vs time, (b) precursor concentration vs time, (c) EDU concentration vs time and (d) anhydride yield vs time.

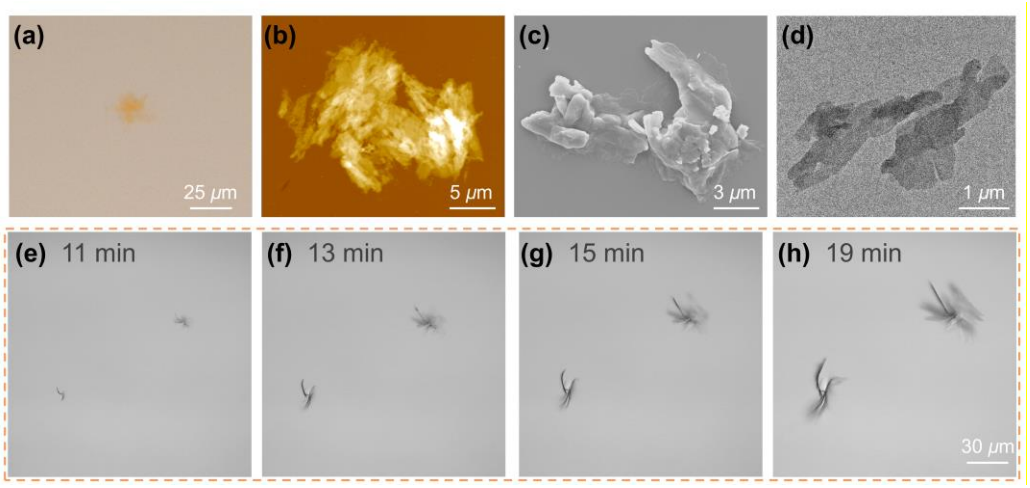

Figure S11. (a−d) Optical, AFM, SEM and TEM micrographs of the coassemblies, respectively. (e−h) Bright-field micrographs of the solution containing precursor (8.0 mM) and AO7 (0.038 mM) after the addition of EDC (16.0 mM, 2.0 equiv.) at different periods.

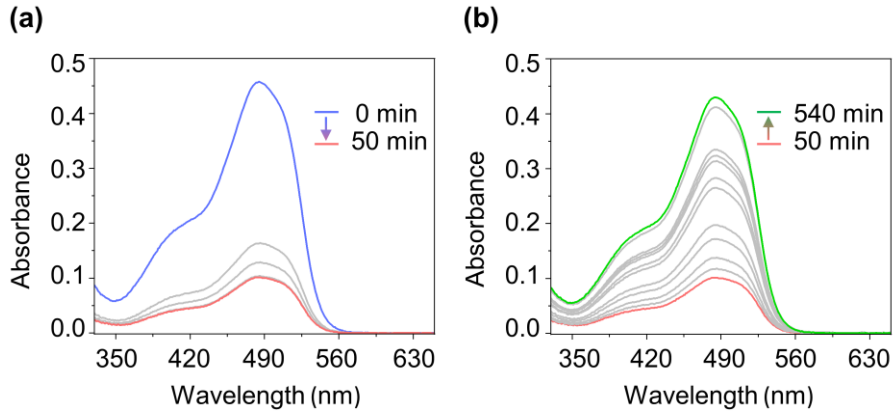

Figure S12. Time-dependent absorption spectra of AO7 in filtrates after removing the assembled AO7 through filtration.

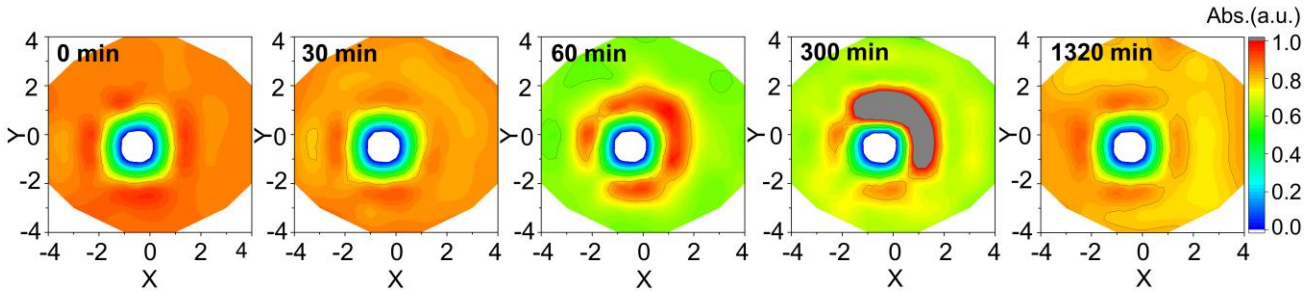

Figure S13. 2D color contours of the absorbance of the entire gel at different periods after injection of EDC (10 μL, 6.3 M) in blank space. Changes in absorbance at 484 nm.

Figure S14. Photograph of the cell after stopping addition of EDC for sufficient time (around 12 h).

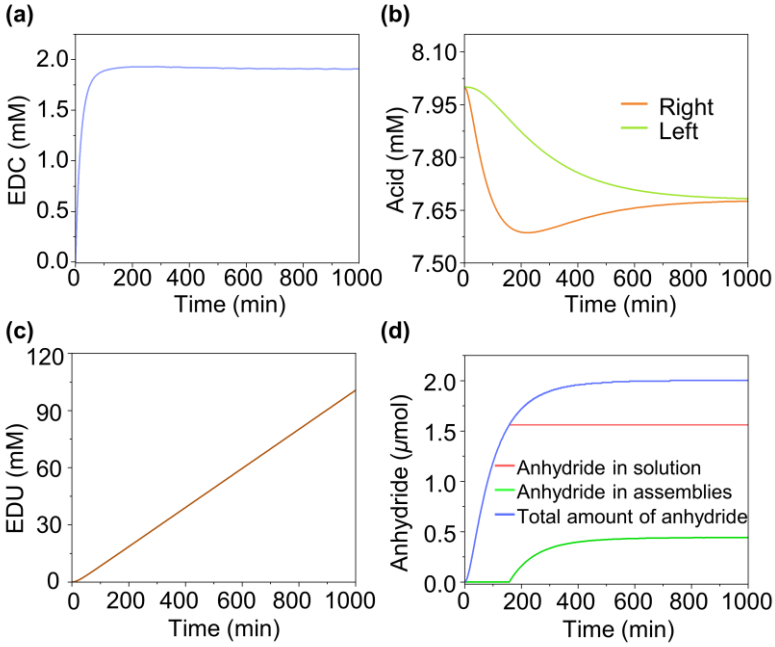

Figure S15. Simulated behaviors of the right side cell during the continuous injection of EDC into the solution of 8.0 mM precursor. (a) EDC concentration vs time, (b) precursor concentration vs time. Right side cell (orange curve) and left side cell (cyan curve), (c) EDU concentration vs time and (d) the amount of anhydride vs time.

Table S1. Total concentration of AO7 in two cells at different times.

Time (min)	Concentration (mM)	
	Left side cell	Right side cell
0	0.038	0.038
180	0.034	0.038
360	0.029	0.040
540	0.027	0.043
720	0.027	0.043

Table S2. *k* values extracted from the fits to the kinetic models are summarized in Figures S2–S4. The parameters are the means of twice replicates and the average parameters are the means of three different concentrations.

EDC	k_0[2b, 3] [min^{-1}]	k_1 [$mM^{-1}\cdot min^{-1}$]	K [mM]	k_2 [min^{-1}]
20 mM	8.1×10^{-4}	0.7×10^{-2}	2.4×10^{2}	1.2×10^{-2}
40 mM	8.1×10^{-4}	0.7×10^{-2}	2.1×10^{2}	1.1×10^{-2}
60 mM	8.1×10^{-4}	0.8×10^{-2}	2.2×10^{2}	1.1×10^{-2}
Average	8.1×10^{-4}	0.7×10^{-2}	2.2×10^{2}	1.1×10^{-2}

Table S3. Relevant parameters in the model of kinetic diffuse phase separation systems.

D	2.3×10^{-5} $m^2\cdot min^{-1}$
x	1.8×10^{-4} m
S	1.3×10^{-4} m^2
V_l	6.0×10^{-3} L
V_r	6.5×10^{-3} L
v ([EDC]=2 M)	1.0×10^{-1} $mM\cdot min^{-1}$
$An_{eq}^{(p)}$	2.4×10^{-1} mM

6. Supporting References

(1) Ruff, Y.; Martinez, R.; Pellé, X.; Nimsgern, P.; Fille, P.; Ratnikov, M.; Berst, F. An Amphiphilic Polymer-Supported Strategy Enables Chemical Transformations under Anhydrous Conditions for DNA-Encoded Library Synthesis, *ACS Comb. Sci.* **2020**, *22*, 120.

(2) (a) Kariyawasam, L. S.; Hartley, C. S. Dissipative Assembly of Aqueous Carboxylic Acid Anhydrides Fueled by Carbodiimides, *J. Am. Chem. Soc.* **2017**, *139*, 11949. (b) Schwarz, P. S.; Laha, S.; Janssen, J.; Huss, T.; Boekhoven, J.; Weber, C. A. Parasitic Behavior in Competing Chemically Fueled Reaction Cycles, *Chem. Sci.* **2021**, *12*, 7554.

(3) Riess, B.; Wanzke, C.; Tena-Solsona, M.; Grotsch, R. K.; Maity, C.; Boekhoven, J. Dissipative Assemblies That Inhibit Their Deactivation, *Soft Matter* **2018**, *14*, 4852.

7. Appendix

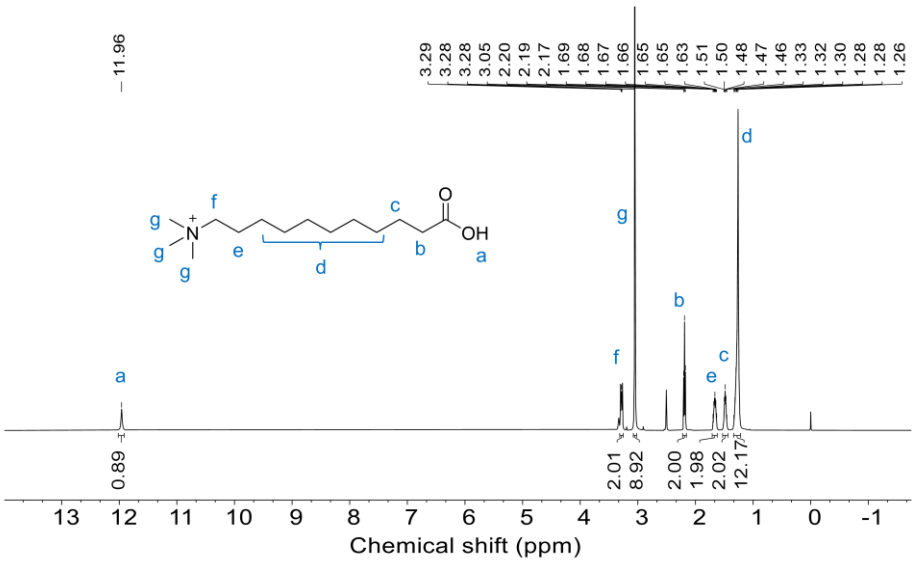

^{1}H NMR spectrum of TMC$_{10}$COOH in DMSO-d_6.